Nanoscale

Accepted Manuscript

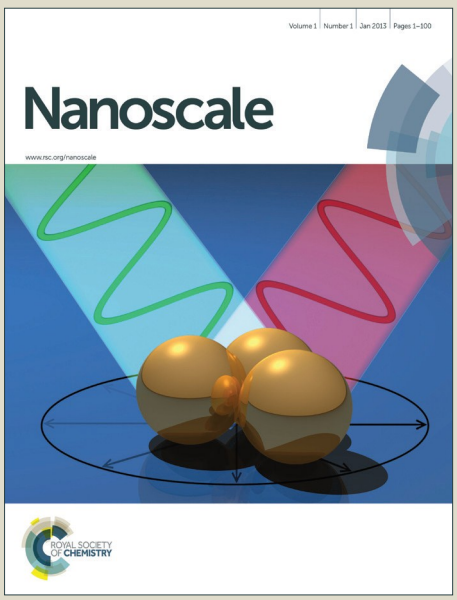

ROYAL SOCIETY OF CHEMISTRY

www.rsc.org/nanoscale

Journal Name

ARTICLE

Title Excitonic Photoluminescence Mechanism and Lasing Action in Band-gap-tunable $CdS_{1-x}Se_x$ Nanostructures

Received 00th January 20xx,
Accepted 00th January 20xx

DOI: 10.1039/x0xx00000x

www.rsc.org/

Jun Dai,[*a,b,†] Pengxia Zhou,[c,†] Junfeng Lu,[a] Hongge Zheng,[b] Jiyuan Guo,[b] Fang Wang,[b] Ning Gu,[a] Chunxiang Xu[a*]

Bandgap tunable semiconductor materials have wide application in integrated-optoelectronic and communication devices. The $CdS_{1-x}Se_x$ ternary semiconductor materials covering green-red bands have been reported previously, but their basic band-gap and optical properties crucial to the performance of the $CdS_{1-x}Se_x$ -based optoelectronic devices have not been deeply understood. In this paper, we theoretically simulated and discussed the feasibility of bandgap-tunable $CdS_{1-x}Se_x$ nanomaterials for designing the wavelength tunable microlasers. Then we fabricated the $CdS_{1-x}Se_x$ nanobelts with their band gap ranging from 2.4 to 1.74 eV by adjusting the composition ratio x in vapor-phase-transport growth process. The temperature-dependent photoluminescence and exciton-related optical constants of the $CdS_{1-x}Se_x$ nanoobelts were carefully demonstrated. Finally, the wavelength-tunable Fabry-Perot lasing in $CdS_{1-x}Se_x$ nanobelts were obtained, and the Fabry-Perot lasing mechanism was numerically simulated by FDTD method. The systematic results on the mechanism of the tunable band gap, exciton properties and lasing of the $CdS_{1-x}Se_x$ nanostructure help us deeply understand its intrinsic optical properties of this material, and will build a strong foundation for future application of green-red wavelength-tunable $CdS_{1-x}Se_x$ microlasers.

Introduction

Band gap engineering is an attractive technique to tune the optoelectronic properties of semiconductor materials and realize wavelength-tunable optoelectronic devices, such as wavelength-tunable lighting-emitting devices and photo-detectors.[1-3] The well known III-V group semiconductors, such as $In_{1-x}Ga_xN$,[4-7] present good band-gap tunability by changing the alloy compositions and have been successfully applied in the lighting industry to yield wavelength-tunable emission. Alloyed II-VI group semiconductor materials, such as $Zn_{1-x}Mg_xO$,[8] $Zn_{1-x}Cd_xO$,[9] $Zn_{1-x}Cd_xSe$,[3] and $CdS_{1-x}Se_x$,[10-13] also have promising application in wavelength-tunable luminescent and photo-detector devices. As an important branch of optics, wavelength-tunable semiconductor laser is always a hot topic because of its wide application in the fields of lighting, laser manufactory, optical data storage and optical communication. Compared to the traditional dye and glass laser materials, the alloyed semiconductor laser materials have more advantages in the integrated optoelectronic devices working in different wavelength band. In addition, II-VI group semiconductor materials are ideal candidates to generate lasing for their high exciton binding energy. As two typical II-VI semiconductor materials, CdS (E_g=2.4 eV) [11, 14] and CdSe (E_g=1.72 eV) [15-16] can be excited to output green and red lasing, respectively. So it is expected to obtain the wavelength-tunable light and lasing between 510 to 720 nm t because its bandgap can be tuned in the range of 1.72-2.4 eV by changing the composition ratio *x* of the $CdS_{1-x}Se_x$ alloy.

Since the first report of ultraviolet ZnO nanowire laser by Yang *et al.* in 2001,[17] micro/nanolaser inspired researchers' enthusiasm for its wide application. As an important lasing band, the green-red lasers have more practical applications in optoelectronic communication and data storage devices. As a result, the CdS and CdSe micro/nanolasers aroused researchers' enthusiasms, and many lasing phenomena from CdS and CdSe nanostructures were successively reported. It is worth noticing that Xiong *et al* reported convincible and perfect Fabry-Perot mode lasing from CdS nanowire in 2012.[14, 18] The stimulated emission from the band-gap tunable $CdS_{1-x}Se_x$ nanowires was observed,[19] however, clear discrete wavelength-tunable Fabry-Perot lasing modes from bandgap tunable $CdS_{1-x}Se_x$ nanostructures have not been reported. Especially neither the theoretical explanation of band gap engineering nor the numerical simulation of lasing mode of the $CdS_{1-x}Se_x$ nanostructures has been investigated to predict and explicate the basic optical properties of this alloyed semiconductor material, and excitonic properties determining the optical characterizations of the $CdS_{1-x}Se_x$ nanostructures have not been studied. So it is of significance to investigate the basic optical mechanisms of the $CdS_{1-x}Se_x$ nanostructure from both theoretical and experimental perspectives.

In this work, the tunable band gap of $CdS_{1-x}Se_x$ were calculated by First-Principle method, the theoretical result

[a] State Key Laboratory of Bioelectronics, Southeast University, Nanjing 210096, China. E-mail:xcxseu@seu.edu.cn
[b] Department of Physics, Jiangsu University of Science and Technology, Zhenjiang 212003, China. E-mail:daijun@just.edu.cn
[c] Department of Physics, Nantong University, Nantong,226019, China.
† These authors contributed equally to this work.

predicts that the ternary semiconductor always maintain the wurtzite structure and presents tunable band gap as the composition ratio of S and Se varies. Then the band-gap-tunable $CdS_{1-x}Se_x$ nanobelts were fabricated by a vapor transport method. The photoluminescence (PL) spectra show that the PL emission wavelength of the samples were successfully tuned from 507nm (2.4 eV, green light) to 710 nm (1.74 eV, red light), the excitonic properties of the band-gap tunable $CdS_{1-x}Se_x$ nanobelts were deeply investigated by temperature-dependent photoluminescence technique. By means of micro-photoluminescence technique, clear wavelength-tunable Fabry-Perot lasing actions from the $CdS_{1-x}Se_x$ nanobelts were observed. Finally the F-P cavity laser modes were deeply investigated by numerical simulation.

Experimental

$CdS_{1-x}Se_x$ samples were synthesized by using a vapor transport method in a tube furnace. A piece of silicon substrate (1 cm × 4 cm) was ultrasonicately cleaned by acetone, ethanol and de-ioned water. A thin layer of gold nanoparticles was sputtered on the substrate by magnetic sputtering method to act as the growth catalyst of $CdS_{1-x}Se_x$. A quartz boat filled with the mixture of CdS and CdSe powder was positioned in the middle of the tube furnace to serve as the source material for growing the $CdS_{1-x}Se_x$. The silicon substrate was placed in the downstream region of the quartz boat. The tube was firstly flushed by Ar gas about 20 minutes, and then evacuated to a base pressure of 2 Pa. To fabricate the $CdS_{1-x}Se_x$ nanobelts, the central temperature of the furnace was heated up from room temperature to 860 ^{o}C with the rate of 10 ^{o}C/min, then kept at 860 ^{o}C for 2 hours. When the furnace temperature reached to 860 ^{o}C, the pressure in the tube was then kept at 300 mtorr under a stable Ar flow of 150 sccm. The as-grown samples were taken out when the furnace temperature was naturally decreased to room temperature. With the above method, pure CdS, CdSe and alloyed $CdS_{1-x}Se_x$ of different composition ratio *x* were fabricated.

The as-grown $CdS_{1-x}Se_x$ nanobelts were characterized by field-emission scanning electron microscopy (FESEM, JEOL JSM-7001F), energy-dispersive X-ray analysis, powder x-ray diffractometer (XRD, Bruker D8 advanced diffractometer with a Cu Ka radiation, λ=1.54056 Å) and high resolution transmission electron microscopy. Photoluminescence spectra were measured by Acton spectrapro 2500i with a 325 nm continuous wavelength He-Cd laser as the excitation source. The lasing action from each $CdS_{1-x}Se_x$ nanobelt was investigated using a home-built micro-photoluminescence system equipped with a femtosecond pulsed laser at wavelength 325 nm as excitation source, the excitation spot was focused to about 10 micrometer on an individual $CdS_{1-x}Se_x$ nanobelt through a 40× objective UV lens, the light emission from an individual $CdS_{1-x}Se_x$ nanobelt was collected by the spectrapro 2500i. The band diagrams of the band gap tunable $CdS_{1-x}Se_x$ were calculated by first-principle method. The F-P cavity laser modes were simulated using FDTD numerical method.

Results and Discussion

To predict and explicate the bandgap tunability of $CdS_{1-x}Se_x$, the first-principles calculations are performed with the Vienna *ab-initio* simulation package code (VASP).[20-21] The exchange correction potential used here is the generalized gradient approximation (GGA). The plane-wave energy cutoff is 500 eV and the Hellman-Feynman forces are 0.01 eV/Å during the optimization. The Monkhorst-Pack *k*-point mesh is 8×4×8. To calculate the cases of x=0, 0.25, 0.5, 0.75 and 1, a supercell including four CdA (A=Se or S) unit cell is chosen to save CPU processing time. To obtain the stable structure of $CdS_{1-x}Se_x$, the energies of two kinds of structures are calculated for $CdS_{0.25}Se_{0.75}$ (or $CdS_{0.75}Se_{0.25}$) and $CdSe_{0.5}S_{0.5}$, respectively. For each x, all of the $CdS_{1-x}Se_x$ atom units with minimum energy have stable wurtzite structures, which are shown in the right panel of Fig. 1. With these stable structures, the band structure and the density of state (DOS) are investigated. The band structure and the DOS are showed in Fig. 1 and Fig. 2, respectively. The results in Fig.1 indicate that E_g of $CdS_{1-x}Se_x$ increases with the x . The energy gap is 0.54, 0.62, 0.78, 0.86 and 1.10 as x=0, 0.25, 0.5, 0.75 and 1 respectively. Usually E_g is evaluated below than the experimental value,[22-23] but it does not affect the ΔE_g [$\Delta E_g = E_{g1}(CdS) - E_{g0}(CdSe)$] qualitatively, regardless of the underestimated E_g.

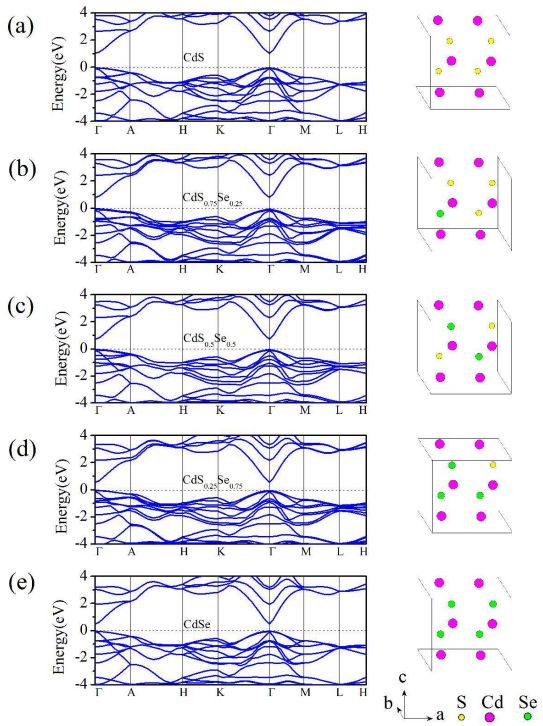

Fig. 1 (a-e) The band structures of the $CdS_{1-x}Se_x$ with x=0, 0.25, 0.5, 0.75 and 1. The right figures denotes the wurtzite crystal structure used in the First-Principle calculation.

To clarify the mechanism of band structure, the atom projected DOS is shown in Fig. 2 shows. Here, the conduction band minimum (CBM) is occupied by the Cd among all *x* cases, while the valence band maximum (VBM) is occupied by the dominant negative ions. For example, the VMB is occupied by Se for $CdS_{0.25}Se_{0.75}$. For the

$CdS_{0.5}Se_{0.5}$, VBM is addressed by both Se and S. By analyzing the orbital projected DOS of each atom, it is found that the VBM and CBM are occupied by the *s* and *p* electrons of corresponding atoms in each case respectively.

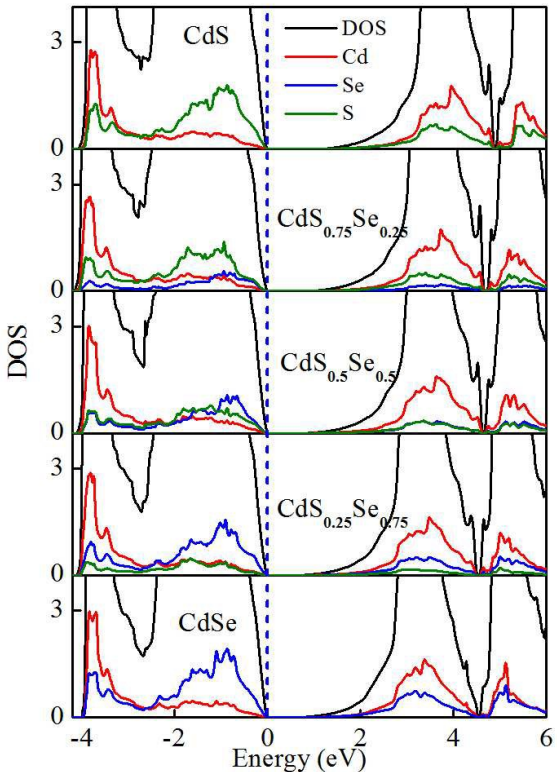

Fig. 2 Density of state of the $CdS_{1-x}Se_x$ with x=0, 0.25, 0.5, 0.75 and 1.

Based on the theoretical result, the $CdS_{1-x}Se_x$ nanostructures were fabricated and investigated. Firstly, pure CdS powder was used as the source material in the vapor phase transport growth process, the CdS nanobelts were obtained. Fig. 3(a-b) shows the scanning electron microscopy (SEM) images of the CdS nanobelts grown on the silicon substrate, the as-grown CdS sample presents a lot of nanobelt, the length of the CdS nanobelts is about tens of micrometers. Fig. 3(b) shows an individual CdS nanobelt with thickness of about 800 nm and width of 9.1 μm. When different amount of CdSe and CdS were mixed to serve as source materials, the $CdS_{1-x}Se_x$ nanobelts with similar morphology and size to that shown in Fig. 3(a) were fabricated under the same growth conditions. The $CdS_{1-x}Se_x$ nanobelt samples with different composition *x* present different colors. Fig. 3(c) shows the optical images of the serial $CdS_{1-x}Se_x$ nanobelt samples with different composition *x* in the daylight. The color gradually changes from yellow (CdS) to dark red (CdSe). Fig. 3(d) shows the SEM of a representative $CdS_{1-x}Se_x$ nanobelt with x=0.25, the elemental mapping images [Fig. 1(e-g)] of the $CdS_{0.75}Se_{0.25}$ nanobelts examined by energy-dispersive X-ray spectroscopy indicates that Cd, S and Se ions distribute homogeneously in the nanobelts. Clear lattice fringes in the HRTEM image [Fig. 3(h)] and SAED pattern [Fig. 3(i)] confirm that the $CdS_{1-x}Se_x$ nanobelt has good crystalline. All of the $CdS_{1-x}Se_x$ samples with different composition *x* present good crystalline structure.

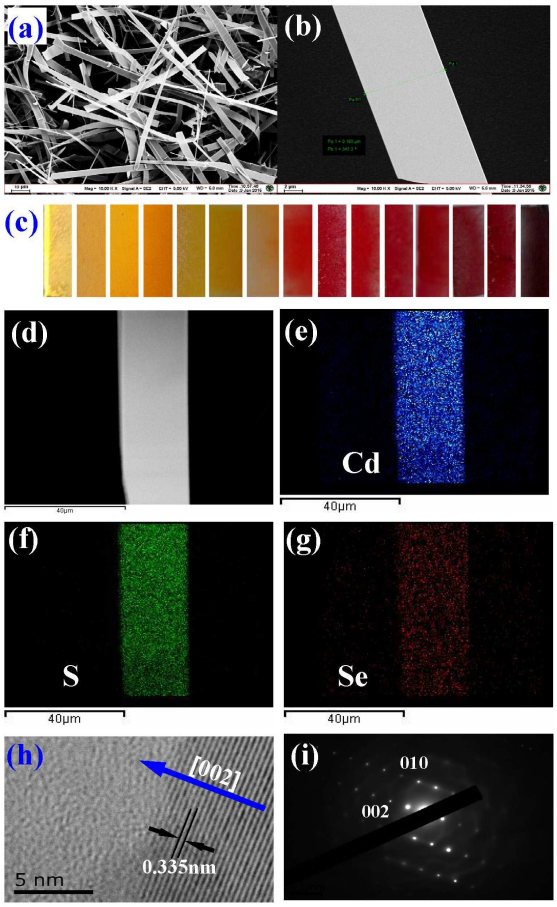

Fig. 3 (a, b) SEM image of CdS nanobelt at different magnifications. (c) Images of the substrates deposited with the $CdS_{1-x}Se_x$ samples, the left one is CdS sample substrate, the right one is CdSe sample, from left to right the composition x increase continuously with the color gradually changes from yellow to dark red. (d) SEM images of an individual $CdS_{0.75}Se_{0.25}$ nanobelt. (e-g) Elements mapping images (Cd, S, Se) of the $CdS_{0.75}Se_{0.25}$ nanobelt. (h, i) HRTEM and SAED patterns of the $CdS_{0.75}Se_{0.25}$ nanobelt.

The X-ray diffraction was employed to characterize the structure of the $CdS_{1-x}Se_x$ samples. In Fig. 4, curve (a) and (i) are the XRD patterns of the CdSe and CdS nanobelt samples, respectively, which indicates that both CdSe and CdS sample have typical wurtzite crystal structures. Curve (b)-(h) are the XRD patterns of the samples with different composition *x*. The (002) peaks from the alloys gradually shifted to higher angle along with the increasing S content in the nanostructures. If the nanobelts were mixtures of CdS and CdSe instead of being alloyed, the resulting XRD patterns would exhibit superposition of the patterns from both of the CdS and CdSe phases. The absence of dual sets of peaks confirms that no phase segregation was formed in the alloy semiconductor samples. According to Bragg's law, the upshift of peak position indicates a decrease in lattice parameter with the increase of S content. From

the continuous shift of the (002) peaks, the c-axis lattice constants of the samples can be calculated. For the ternary $CdS_{1-x}Se_x$ compounds, the lattice parameters obey a linear dependence on the composition x according to Vegard's law: $c(x)=xc_{CdSe}+(1-x)c_{CdS}$, where c_{CdS}, c_{CdSe} and $c(x)$ are the c-axis lattice constants of the wurtzite CdS, CdSe and $CdS_{1-x}Se_x$, respectively. As a result, the composition x of the samples can be determined by Vegard's law using the lattice constants deduced from the XRD patterns. As shown in Figure 2, the composition x were labelled. The determined compositions are in good agreement with the result of the optical band gaps discussed in the next section.

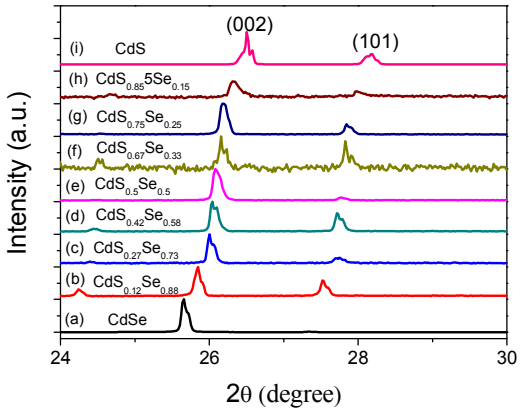

Fig. 4 XRD patterns of the $CdS_{1-x}Se_x$ samples with various composition x.

Fig. 5 shows the normalized room temperature PL spectra of the $CdS_{1-x}Se_x$ samples. Curve (a) and (h) are the PL spectra for pure CdS and CdSe nanobelts, respectively. Curves (b-g) are the PL spectra of the $CdS_{1-x}Se_x$ nanobelts with x ranging from 0.1 to 0.9. All of the PL emission bands present a single peak with their center wavelength varying from 512 to 708 nm, which cover the green-red visible wavelength region. The upper insets of Fig. 5 show the images of three typical samples (CdS, $CdS_{0.75}Se_{0.25}$, $CdS_{0.44}Se_{0.56}$) under excitation of 325 nm He-Cd laser. The green, yellow and red light emission can be observed from the three samples. Pure CdS nanobelt powder sample emits intense green light, $CdS_{0.75}Se_{0.24}$ and $CdS_{0.44}Se_{0.56}$ emit yellow and red light, respectively. Pure CdSe sample emits dark red light which is not sensitive to naked eye. Single emission peak for each sample indicated that only the near-band edge exciton recombination occurred, and no low-energy sub-bands related to defects formed in the samples. Such a continuous tunability of the PL emission peaks further confirms the well crystallization of alloyed $CdS_{1-x}Se_x$ rather than the formation of segregated CdS and CdSe nanobelts. On the other hand, the tunable PL result indicated that the band gap (E_g=1240/λ) of the $CdS_{1-x}Se_x$ nanobelts can be tuned by changing the composition x, this agreed well with the numerical calculation result shown in Fig. 1. As shown in Fig. 6, the determined bandgap of the $CdS_{1-x}Se_x$ nanobelts nonlinearly depends on alloy composition x with a fitted quadratic function as follows,

$$E_g(CdS_{1-x}Se_x)=xE_g(CdS)+(1-x)\,E_g(CdSe)-bx(1-x). \quad (1)$$

Where $E_g(CdS_{1-x}Se_x)$, $E_g(CdS)$ and $E_g(CdSe)$ are the energy gaps of $CdS_{1-x}Se_x$, CdS (2.4 eV) and CdSe(1.72 eV), respectively. The least-squared fit yields an optical bowing constant b=0.54±0.01 eV which indicates an upward bowing of the bandgap for the $CdS_{1-x}Se_x$ nanostructures, the E_g-x relationship in Fig. 6 agrees well with the previous report [13].

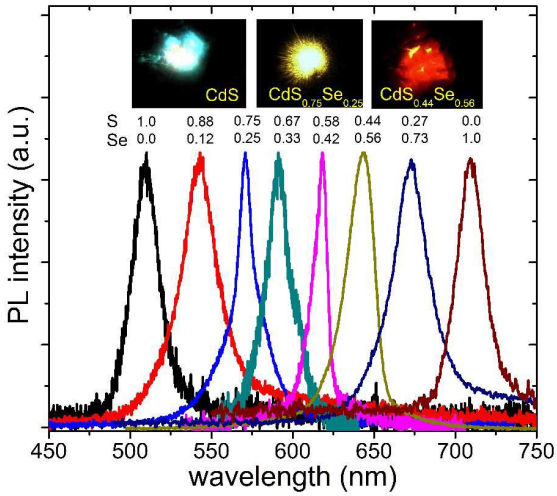

Figure 5. PL spectra of the $CdS_{1-x}Se_x$ samples with different Se contents. The insets show the photographs of typical emission colors from the obtained alloyed CdS, $CdS_{0.75}Se_{0.24}$, $CdS_{0.44}Se_{0.56}$ samples excited by UV 325 nm irradiation.

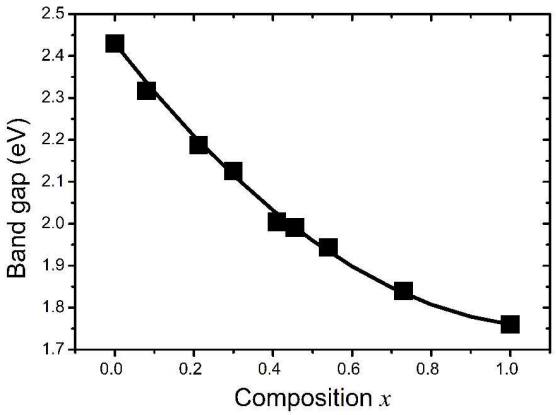

Figure 6. Energy gap–composition correlation of $CdS_{1-x}Se_x$ samples, where the data points represent the value extracted from their respective PL. The solid line is the fitting of the experimental results.

The excitonic PL behaviors of CdS [24-25] and CdSe [15] nanostructures have been investigated previously. However, the exciton recombination mechanism and exciton activation energy of the band gap tunable $CdS_{1-x}Se_x$ sample have not been reported systematically. It is of significance to know these exciton properties

of $CdS_{1-x}Se_x$ for corresponding optoelectronics device design. Figure 7 shows the temperature-dependent PL spectra from three $CdS_{1-x}Se_x$ nanobelts with different *x*. The temperature-dependent PL spectra of $CdS_{0.7}Se_{0.3}$ nanobelts are shown in the Fig. 7(a), two emission peaks locating at 559.6 nm (2.215 eV) and 564.3 nm (2.197 eV) can be distinguished at 10 K, with the temperature increasing, the two peaks shift to the long wavelength, and the intensity of the peak with high energy becomes dominant in the spectra. We can conclude that the peak at 559. 6 nm is originated from free exciton and the peak at 564.3 nm is originated from DX. Fig. 7(b) shows the temperature-dependent PL spectra of $CdS_{0.6}Se_{0.4}$ sample. Only an emission band can be observed in the PL spectra, the single emission band can be attributed to the free exciton recombination emission. The temperature-dependent PL spectra of $CdS_{0.23}Se_{0.77}$ sample are shown in Fig. 7(c), where three emission peaks at 623.1 nm (1.991 eV), 644.5 nm (1.924 eV) and 677.9 nm (1.831 eV) can be distinguished at 10 K, and the three emission peaks gradually shifts to long wavelength side, and mixed to a single emission band at 120 K because the band broadening due to thermal effect. The emission band at 644.5 nm has a stronger intensity than the other two emission bands at low temperature, which can be attributed to the dominant free exciton recombination emission band. However, the origination of two other emission bands at low temperature is not clear. Here we speculate that the substitution doping of S in the CdSe is a little imhomogeneous, which can be confirmed by its XRD pattern [curve (c) in Fig. 4]. A little the imhomogeneous doping resulted in a non-symmetrical (002) diffractive peak which looks like have two sub-peaks, so we suggest that the three PL bands in Fig. 7(c) are caused by a little difference of the bandgap in different micro-areas induced by the tiny imhomogeneous doping. Only at low temperature, the little difference bandgap in different areas can be presented in the PL spectra, the thermal effect can broaden the emission with the temperature increasing, so only a main emission band at 678 nm can be observed when the temperature is higher than 240 K.

The insets of the Figure 7 (a-c) show the variations in integrated PL intensity of FX as a function of 1/*T*. Then integrated PL intensity can be well reproduced by the Arrhenius equation[26]:

$$I_{(T)} = \frac{I_{(0)}}{1 + ce^{-E_a/k_B T}} \quad (2)$$

where E_a is the activation energy for thermal activation process, k_B is Boltzmann constant, and *c* is the relative ratio of nonradiative recombination. The fundamental band gap as a function of temperature can be well fitted with empirical equation describing the semiconductor band gap temperature evolution, viz. Varshni equation[24]:

$$E(T) = E(0) - \frac{\alpha T^2}{T + \beta} \quad (3)$$

where E(0) is the band gap at 0 K; α and β are constants related to materials which are deemed as Varshni's coefficients. Especially, α stands for the linear shift of *E*(*T*) at high temperature and β represents the quadratic variation of E(*T*) at low temperature. For the three $CdS_{1-x}Se_x$ samples with different bandgap values, the fitted band gap at 0 K, activation energy, α and β were listed in the table I. For the $CdS_{1-x}Se_x$ samples, they have different optical constants**.** For the same materials fabricated at different conditions, they present different excitonic optical constants which are strongly related to the intrinsic crystal properties[24-25, 27-28].

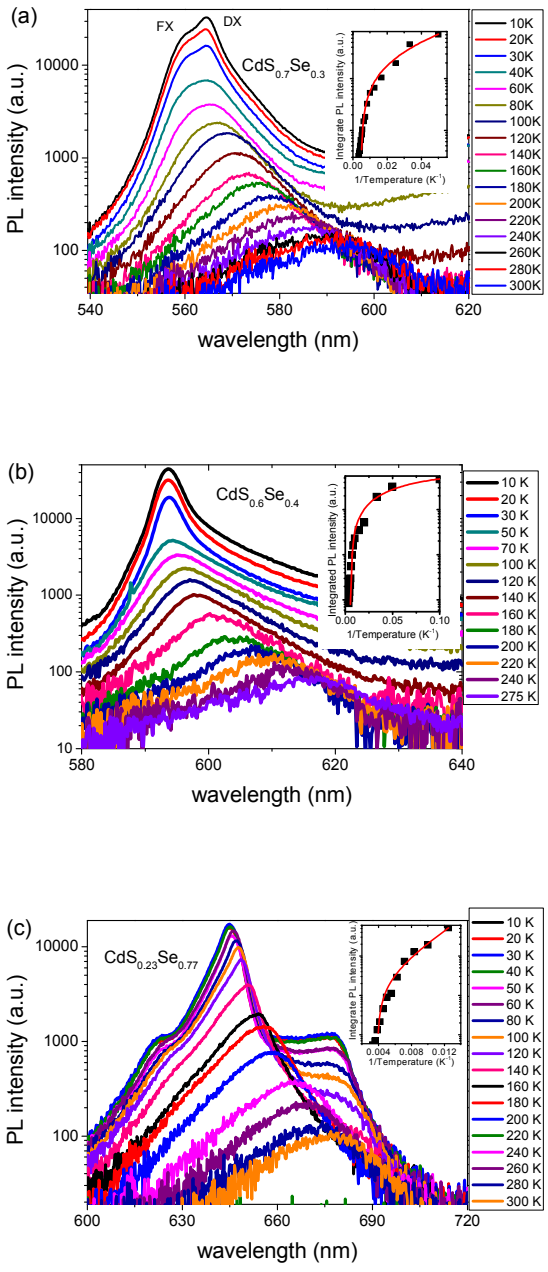

Fig. 7 (a-c). Temperature-dependent PL spectra of the $CdS_{1-x}Se_x$ nanobelts with different x. The insets are the integrated PL intensity with 1/T.

Table I. Exciton-related optical constants of $CdS_{1-x}Se_x$ samples.

	$CdS_{0.7}Se_{0.3}$	$CdS_{0.6}Se_{0.4}$	$CdS_{0.25}Se_{0.75}$
E(0) (eV)	2.216	2.088 eV	1.923 eV
E_o (meV)	48.41	58.62	65
α (meV/K)	6.5	4.5	9
β (K)	160	200	260

As shown in Figure 3, the $CdS_{1-x}Se_x$ nanobelts have regular belt structure with its width much longer than the wavelength, therefore Fabry-Perot mode optical feedback or lasing can be formed between two sides. The $CdS_{1-x}Se_x$ nanobelts were then dispersed on the silicon substrate, and the micro-photoluminescence technique was employed to excite an individual $CdS_{1-x}Se_x$ nanobelt to observe the Fabry-Perot lasing action. Fig. 8 shows the emission spectra from $CdS_{1-x}Se_x$ nanobelts with different band gap under excitation power of 600 KW/cm^2, the emission bands have much narrower band width than that of the PL emission shown in Figure 5, and discrete sharp emission peaks can be found from the spectra. The narrow band width and multiple peak structure indicate the formation of the lasing action. As a representative example, Fig. 9 shows the evolution of lasing emission from a single $CdS_{0.67}Se_{0.33}$ nanobelt with width of about 20.6 μm. As shown in the Fig. 9(a), when the average excitation power density was 300 KW/cm^2, only an emission band centered at 587.5 nm can be observed. When the average excitation power density increased to 350 KW/cm^2, seven sharp peaks with their peak spacing of 1.1 nm appeared on the emission band, and the intensity of the emission peaks increased quickly with the increasing excitation intensity. The inset of Fig. 9(a) shows the relationship between the emission intensity and the excitation power density, which indicates that the lasing action was formed in the single $CdS_{0.67}Se_{0.33}$ nanobelt. The output-input relationship presents two different linear regions, the intersection point of the two linear regions can be estimated as the lasing threshold. Fig. 9(b) shows the SEM image of the nanobelt, the Fabry-Perot mode optical feedback between two sides is denoted. Figure 9(c) shows the image of the nanobelt at lasing action, we can find that the light was emitted from the two sides, which obviously indicates the formation of the Fabry-Perot lasing action in the nanobelt.

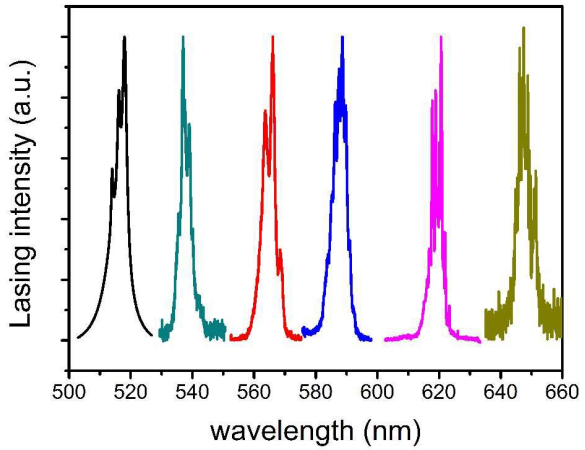

Fig. 8 Lasing spectra of $CdS_{1-x}Se_x$ nanobelts excited by a femtosecond laser at excitation power of 600 KW/cm^2.

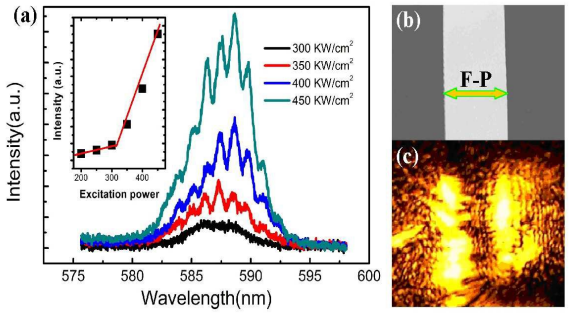

Figure 9. (a) Lasing spectra of single $CdS_{1-x}Se_x$ (yellow) nanobelt at different excitation power densities. The inset show the input-output relationship. (b-c) The images of the unexcited and excited nanobelt, respectively.

To confirm the F-P mode lasing mechanism, the experimental and theoretical lasing mode spacings are compared. For the F-P cavity, the mode spacing $\Delta\lambda$ can be deduced by the equation:

$$\Delta\lambda = \frac{\lambda^2}{2L(n - \lambda\frac{dn}{d\lambda})} \quad (4)$$

n is the refractive index at resonance wavelength, λ is the resonance wavelength, and *L* is the length of the laser cavity, and the chromatic dispersion $dn/d\lambda$=-0.008nm^{-1}. According to the experimental mode spacing, we can deduce the cavity length *L* of the CdS nanobelt is about 22 um, which is very close to the real length shown in the Fig. 9(b). So we confirm that F-P lasing is formed in the nanobelt. The FWHM of lasing peak is about 1.6 nm, we can estimate the Q factor is about 320. In addition, we calculated the theoretical quality factor of the Fabry-Perot microlaser according to the equation,

$$Q = \frac{2\pi nL}{\lambda(1-R)} \quad (5)$$

Where *R* is the reflectivity, $R=(n-1)^2/(n+1)^2$=19.7%, *Q* is calculated as 780. The experimental lasing quality factor is much lower than the theoretical one. Because the nanobelt has a very thin thickness, the optical confinement is poor, and the quality factor will be decreased.

To further demonstrate the lasing action in the rectangular cross section, we simulated the optical resonance feedback in the rectangular, as shown in Figure 10. A Gaussian light beam with FWHM of 8 nm is selected to transport between the two sides in the nanobelt cavity. The light intensity distribution (Figure 10) shows that the light is mainly emitted from two side boundaries, meanwhile we can find that the intensity is not uniform in the nanobelt because Fabry-Perot optical resonance induces the resonant optical pattern. Where the points of highest light intensity in the cavity correspond to the optical resonance antinodes, and those points of lowest light intensity are the positions of optical

resonance nodes. The light output at two side boundaries in Figure 10 is very similar to that in Figure 9(c), which proves that the Fabry-Perot lasing modes are formed in the nanobelt cavity.

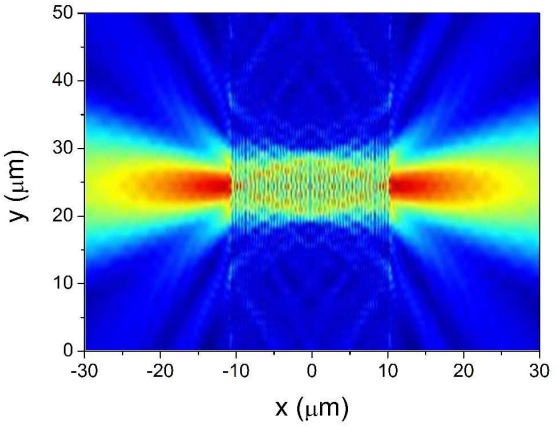

Figure 10. The light intensity distribution of the nanobelt laser cavity.

Conclusions

CdS1-xSex nanobelts with the composition ratio x ranging from 0 to 1 were fabricated by vapor phase transport method. Systematical characterizations were performed to determine the composition and crystal structure of the $CdS_{1-x}Se_x$ nanobelts. The band gap of $CdS_{1-x}Se_x$ nanobelts can be tuned from 2.4 to 1.74 eV when the composition ratio x changes from 0 to 1. To explain the tunable band gap mechanism, the band diagrams of the $CdS_{1-x}Se_x$ was simulated by first-principle method. Under the excitation of 325 nm line of a femtosecond pulsed laser, wavelength-tunable lasing in $CdS_{1-x}Se_x$ nanobelts were obtained by the confocal micro-photoluminescence technique, then the light distribution in the nanobelt cavity were numerically simulated by FDTD method, the theoretical and experimental results confirmed that the lasing in $CdS_{1-x}Se_x$ nanobelts was Fabry-Perot mode. The result indicated that the $CdS_{1-x}Se_x$ nanostructures can be used as ideal optoelectronic material for wavelength-tunable laser diodes.

Acknowledgements

This work was supported by NSFC (11104119 and 11304128), 973 Program (2013CB932903), Jiangsu Province Natural Science Fund (SBK2015021741), Open funding of state key laboratory of bioelectronics, Qinglan Project of Jiangsu Province, China Postdoctoral Science Foundation (2014M551485).

Notes and references

1 Z. Deutsch, O. Schwartz, R. Tenne, R. Popovitz-Biro and D. Oron, Nano Lett., 2012, **12**, 2948-2952.
2 D. Q. Fang, A. L. Rosa, T. Frauenheim and R. Q. Zhang, Appl. Phys. Lett., 2009, **94**, 073116.
3 J. Xu, X. Yang, H. K. Wang, X. Chen, C. Y. Luan, Z. X. Xu, Z. Z. Lu, V. A. L. Roy, W. J. Zhang and C. S. Lee, Nano Lett., 2011, 11, 4138-4143.
4 T. Kuykendall, P. Ulrich, S. Aloni and P. Yang, Nature. Mater., 2007, 6, 951-956.
5 H. P. T. Nguyen, S. Zhang, K. Cui, X. Han, S. Fathololoumi, M. Couillard, G. A. Botton and Z. Mi, Nano Lett., 2011, 11, 1919-1924.
6 K. Okamoto, I. Niki, A. Shvartser, Y. Narukawa, T. Mukai and A. Scherer, Nature. Mater., 2004, 3, 601-605.
7 R. H. Kim, D. H. Kim, J. L. Xiao, B. H. Kim, S. I. Park, B. Panilaitis, R. Ghaffari, J. M. Yao, M. Li, Z. J. Liu, V. Malyarchuk, D. G. Kim, A. P. Le, R. G. Nuzzo, D. L. Kaplan, F. G. Omenetto, Y. G. Huang, Z. Kang, J. A. Rogers, Nature. Mater., 2010, 9, 929-937.
8 D. Y. Jiang, C. X. Shan, J. Y. Zhang, Y. M. Lu, B. Yao, D. X. Zhao, Z. Z. Zhang, D. Z. Shen and C. L. Yang, J. Phys. D: Appl. Phys., 2009, 42, 025106.
9 S. Kalusniak, S. Sadofev, J. Puls, F. Henneberger, Laser & Photonics Reviews., 2009, 3, 233-242.
10 J. Xu, X. Zhuang, P. Guo, Q. Zhang, W. Huang, Q. Wan, W. Hu, X. Wang, X. Zhu, C. Fan, Z. Yang, L. Tong, X. Duan and A. Pan, Nano Lett., 2012, 12, 5003-5007.
11 P. Guo, X. Zhuang, J. Xu, Q. Zhang, W. Hu, X. Zhu, X. Wang, Q. Wan, P. He, H. Zhou and A. Pan, Nano Lett., 2013, 13, 1251-1256.
12 J. P. Kim, J. A. Christians, H. Choi, S. Krishnamurthy and P. V. Kamat, J. Phys. Chem. Lett., 2014, 5, 1103-1109.
13 J. Pan, M. I. B. Utama, Q. Zhang, X. F. Liu, B. Peng, L. M. Wong, T. C. Sum, S. J. Wang and Q. H. Xiong, Adv. Mater., 2012, 24, 4151-4156.
14 X. Liu, Q. Zhang, J. N. Yip, Q. H. Xiong and T. C. Sum, Nano Lett., 2013, 13, 5336-5343.
15 R. Chen, M. I. B. Utama, Z. Peng, B. Peng, Q. H. Xiong and H. D. Sun,, Adv. Mater., 2011, 23, 1404-1408.
16 G. Li, T. Zhai, Y. Jiang, Y. Bando, D. Golberg, J. Phys. Chem. C. 2011, 115, 9740-9745.
17 M. H. Huang, S. Mao, H. Feick, H. Yan, Y. Wu, H. Kind, E. Weber, R. Russo and P. Yang, Science. 2001, 292, 1897-1899.
18 X. Liu, Q. Zhang, Q. H. Xiong and T. C. Sum, Nano Lett., 2013, 13, 1080-1085.
19 A. L. Pan, W. C. Zhou, E. S. P. Leong, R. B. Liu, A. H. Chin, B. S. Zou, C. Z. Ning, Nano Lett., 2009, 9, 784-788.
20 G. Kresse and J. Hafner, Phy. Rev. B 1993, 47, 558.
21 G. K. J. Furthmuller, Phy. Rev. B 1996, 54, 11169-11186
22 X. D. Liu, T. Xing, Solid. State. Commun., 2014, 187, 72-76.
23 N. A. Noor, W. Tahir, F. Aslam and A. Shaukat, Physica B., 2012, 407, 943-952.
24 B. Liu, R. Chen, X. L. Xu, D. H. Li, Y. Y. Zhao, Z. X. Shen, Q. H. Xiong, H. D. Sun, J. Phys. Chem. C. 2011, 115, 12826-12830.
25 C. Hu, X. Zeng, J. Cui, H. Chen and J. Lu, J. Phys. Chem. C. 2013, 117, 20998-21005.
26 X. H. Gu, G. Qian, J. Fu and P. K. Chu, Appl. Phys. Lett., 2008, 93, 203117.
27 S. K. Mohanta, S. Tripathy, X. H. Zhang, D. C. Kim, C. B. Soh, A. M. Yong, W. Liu and H. K. Cho, Appl. Phys. Lett., 2009, 94, 041901.
28 I. Musa, F. Massuyeau, L. Cario, J. L. Duvail, S. Jobic, P. Deniard and E. Faulques, Appl. Phys. Lett. 2011, 99, 243107.

Table of contents

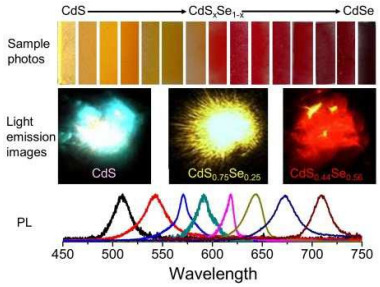

We fabricated $CdS_{1-x}Se_x$ nanobelts with their band-gap ranging from 2.4 to 1.74 eV, excitonic photoluminescence and lasing were systematically investigated.